HHS Public Access

Author manuscript

Cancer Res. Author manuscript; available in PMC 2020 June 01.

Published in final edited form as:

Cancer Res. 2019 June 01; 79(11): 2812–2820. doi:10.1158/0008-5472.CAN-18-3592.

N^6-methylation of adenosine (m^{6}A) of *FZD10* mRNA contributes to PARP inhibitor resistance

Takeshi Fukumoto[1], **Hengrui Zhu**[1], **Timothy Nacarelli**[1], **Sergey Karakashev**[1], **Nail Fatkhutdinov**[1,2], **Shuai Wu**[1], **Pingyu Liu**[1], **Andrew V. Kossenkov**[3], **Louise C. Showe**[3,4], **Stephanie Jean**[5], **Lin Zhang**[6], and **Rugang Zhang**[1,*]

[1]Gene Expression and Regulation Program, The Wistar Institute, Philadelphia, PA 19104, USA

[2]Kazan Federal University, Kazan, Russia.

[3]Center for Systems and Computational Biology, The Wistar Institute, Philadelphia, PA 19104, USA

[4]Molecular and Cellular Oncogenesis Program, The Wistar Institute, Philadelphia, PA 19104, USA

[5]Helen F. Graham Cancer Center & Research Institute, Newark, DE 19713, USA.

[6]Department of Obstetrics and Gynecology, University of Pennsylvania Perelman School of Medicine, Philadelphia, PA 19104, USA.

Abstract

Despite the high initial response rates to PARP inhibitors (PARPi) in *BRCA*-mutated epithelial ovarian cancers (EOC), PARPi resistance remains a major challenge. Chemical modifications of RNAs have emerged as a new layer of epigenetic gene regulation. N^6-methyladenosine (m^{6}A) is the most abundant chemical modification of messenger RNA (mRNA), yet the role of m^{6}A modification in PARPi resistance has not previously been explored. Here we show that m^{6}A modification of *FZD10* mRNA contributes to PARPi resistance by upregulating the Wnt/β-catenin pathway in *BRCA*-mutated EOC cells. Global m^{6}A profile revealed a significant increase in m^{6}A modification in *FZD10* mRNA, which correlated with increased *FZD10* mRNA stability and an upregulation of the Wnt/β-catenin pathway. Depletion of FZD10 or inhibition of the Wnt/β-catenin sensitizes resistant cells to PARPi. Mechanistically, downregulation of m^{6}A demethylases FTO and ALKBH5 was sufficient to increase *FZD10* mRNA m^{6}A modification and reduce PARPi sensitivity, which correlated with an increase in homologous recombination activity. Moreover, combined inhibition of PARP and Wnt/β-catenin showed synergistic suppression of PARPi-resistant cells *in vitro* and *in vivo* in a xenograft EOC mouse model. Overall, our results show that m^{6}A contributes to PARPi resistance in BRCA-deficient EOC cells by upregulating the Wnt/β-catenin pathway via stabilization of FZD10. They also suggest that inhibition of the Wnt/β-catenin pathway represents a potential strategy to overcome PARPi resistance.

*Correspondence should be addressed to: **Rugang Zhang, Ph.D.**, Gene Expression and Regulation Program, The Wistar Institute, 3601 Spruce Street, Philadelphia, PA 19104, rzhang@wistar.org.

Disclosure of Potential Conflicts of Interests: The authors declare no competing financial interests.

Introduction

Poly(ADP-ribose) polymerase inhibitors (PARPi) are synthetically lethal in cells with a dysfunctional homologous recombination (HR) pathway such as those with *BRCA1/2* mutations (1). PARP inhibitors such as Olaparib have been approved by the FDA for treating *BRCA1/2*-mutated epithelial ovarian cancer (EOC) with substantial clinical benefits (1,2). However, the mechanisms of resistance to PARPi remain to be fully elucidated.

Wnt signaling is initiated by binding of the Wnt ligand to its cognate frizzled receptor (3,4). A key feature of the canonical Wnt signaling is stabilization of the downstream effector β-catenin. β-catenin translocation to nuclei promotes the expression of β-catenin target genes such as *CCND1* and *FOSL1* through partnering with the TCF/LEF transcription factors (5). However, the role of Wnt/β-catenin signaling in PARPi sensitivity in *BRCA1/2*-mutated cancers remains to be elucidated.

N^6-methyladenosine (m^6A) is the most prevalent modification that occurs in the messenger RNAs (6). The modification is catalyzed by the m^6A methyltransferase “writers” and can be removed by demethylase “erasers”. The core m^6A writer complex includes methyltransferase-like 3 (METTL3) and methyltransferase-like 14 (METTL14) (6). m^6A erasers include fat mass and obesity-associated (FTO) and AlkB homolog 5 (ALKBH5) demethylases (6). The distribution of m^6A is not random across the transcriptome. It is enriched around stop codons, in 3’ untranslated regions (UTRs), within internal long exons and 5’-UTRs (7–10). The specific fate of m^6A modified mRNA is often dependent on specific m^6A readers. For example, HuR (11) and IGF2BPs (12) enhance the stabilization of the m^6A modified mRNA, while YTHDF2 contributes to the decay of m^6A modified mRNA (13). m^6A modification is linked to a variety of biological processes that are important for cancer development and progression (14). Here we show that m^6A modification of *FZD10* mRNA contributes to PARPi resistance by upregulating the canonical Wnt/β-catenin signaling in *BRCA1/2*-mutated ovarian cancer cells.

Materials and Methods

Cell lines, culture conditions and transfection.

The ovarian cancer cell line PEO1 was cultured in RPMI 1640 (Corning Life Sciences) supplemented with 10% fetal bovine serum (FBS; Sigma-Aldrich) and 1% penicillin/streptomycin at 37°C supplied with 5% CO2. PARPi resistant PEO1 cells were published previously (15) and were developed by a continuous stepwise exposure to increasing concentration of the PARP inhibitor Olaparib. The resistant PEO1 cells were maintained and passaged in 5 μM Olaparib. The ovarian cancer cell line UWB1.289 was cultured in 1:1 RPMI 1640/Mammary Epithelial Growth Medium (Lonza, Cat. No. CC-3150) supplemented with 3% FBS at 37°C supplied with 5% CO2. Viral packing cell 293FT was cultured in Dulbecco’s modified Eagle’s medium (DMEM) with 10% FBS and 1% penicillin/streptomycin at 37°C supplied with 5% CO_2. Cell lines were obtained from ATCC and were re-authenticated by The Wistar Institute Genomics Facility at the end of experiments using short tandem repeat profiling using AmpFLSTR Identifiler PCR Amplification Kit (Life Technologies). Mycoplasma testing was performed using LookOut Mycoplasma PCR

detection (Sigma-Aldrich) every month. Transfection was performed using Lipofectamine 2000 (Life Technologies) following the manufacturer's specifications. Each of the experiments was performed in triplicate in three independent experimental repeats unless otherwise stated.

Reagents and antibodies.

Olaparib (Cat. No: S1060), Rucaparib (Cat. No: S1098), Nirapalib (Cat. No: S2741) and XAV939 (Cat. No: S1180) were purchased from Selleckchem. Pyrvinium pamoate (Cat. No: 1592001) was purchased from Sigma-Aldrich. The following antibodies were obtained from the indicated suppliers: anti-β-actin (Sigma-Aldrich, Cat. No. A5441, 1:10,000), anti-Vinculin (Santa Cruz, Cat. No. sc-25336, 1:1000), anti-GAPDH (Millipore, Cat. No. MAB374, 1:10,000), anti-Ki67 (Cell Signaling, Cat. No. 9449, 1:500), anti-Cleaved caspase 3 (Cell Signaling, Cat. No. 9661, 1:1000 for western blot and 1:50 for IHC), anti-cleaved PARP p85 (Promega, Cat. No. G7341, 1:1000), anti-FZD10 (Santa Cruz, Cat. No. sc-33510, 1:2000), anti-BRCA1 (Milliporel, Cat. No. 07–434, 1:1000), and anti-BRCA2 (Bethyl, Cat. No. A303–434A, 1:1000), anti-β-catenin (BD Biosciences, Cat. No. 610153, 1:1000), anti-HA (Cell Signaling, Cat. No. 2367, 1:1000) and anti-V5 (Thermo Fisher, Cat. No. R960–25, 1:1000).

Immunoblotting.

Protein was isolated with RIPA buffer (50mM Tris pH 8.0, 150mM NaCl, 1% Triton X-100, 0.5% sodium deoxycholate and 1mM PMSF). Protein concentration was measured using Bradford assay. Protein was separated on a SDS-PAGE and transferred to polyvinylidene fluoride membrane (Millipore). Membranes were blocked with 5% non-fat milk (Bio-Rad) in TBS/0.1% Tween 20 (TBST), and then incubated sequentially with primary and secondary antibodies.

Chromatin fractionation was performed as described previously (16). Briefly, cells were washed once by PBS, trypsinized and centrifuged at 1,000 rpm. The pellets were resuspended in 300 μl buffer A: 10 mM Hepes-KOH, pH 8.0, 10 mM KCl, 1.5 mM $MgCl_2$, 0.34 M sucrose, and 10% glycerol, pH 7.5, plus the EDTA-free Protease Inhibitor Cocktail (Roche), 1 mM DTT, 0.1 mM PMSF, 0.1% Triton X-100. Cells were incubated on ice for 5 min and pelleted at 1,300 *g* for 4 min at 4°C. The supernatant was obtained as the cytoplasmic fraction. The pellet was washed once in buffer A and then resuspended in 300 μl buffer B: 3 mM EDTA, pH 8.0, and 0.2 mM EGTA, pH 8.0, plus the EDTA-free Protease Inhibitor Cocktail, 1 mM DTT, and 0.1 mM PMSF. Samples were incubated on ice for 30 min and then centrifuged at 1,700 *g* for 4 min at 4°C. The supernatant was obtained as the nuclear fraction and resuspended in 1× sample buffer.

Cycloheximide chase analysis.

Cycloheximide was added to cells, and then the cells were collected at 0, 4, 8, 16 and 24 hours post treatment. The protein levels of FZD10 were examined by immunoblotting.

Lentivirus packaging and infection.

Lentivirus was packaged using the Virapower Kit from Invitrogen according to the manufacturer's instructions as described previously (17). HEK293FT cells were transfected by Lipofectamine 2000. Lentivirus was harvested 48 hours post-transfection. Cells infected with viruses encoding the puromycin-resistance gene were selected using 1 μg/ml puromycin or 10 μg/ml blasticidin. pLKO.1-shFZD10 (1, TRCN0000008315; 2, TRCN0000008316), pLKO.1-shALKBH5 (1, TRCN0000064783; 2, TRCN0000064787), pLKO.1-shHuR (1, TRCN0000017273; 2, TRCN0000017274), pLKO.1-shIGF2BP2 (1, TRCN0000149224; 2, TRCN0000148718) were obtained from the Molecular Screening Facility at the Wistar Institute. pLKO.1-shFTO (TRCN0000246250) and pLKO.1-sh *YTHDF2* (1, TRCN0000254410; 2, TRCN0000254411) were purchased from Sigma-Aldrich. For FTO and ALKBH5 expression vector, pLX304-FTO (clone ID# ccsbBroad304_15979) was obtained from the Molecular Screening Facility at the Wistar Institute. The pLenti-ALKBH5 (clone ID# NM_017758) was purchased from Applied Biological Materials Inc.

Quantitative RT-PCR (qRT-PCR).

RNA was extracted using TRIzol (Invitrogen) according to manufacturer's instruction, and then DNase treatment (RNeasy columns by Qiagen) was performed. RNA expression was determined using the iTaq Universal SYBR Green One-step kit (Bio-Rad Laboratories) on the QuantStudio 3 Real-Time PCR System (Thermo Fisher).

The primers sequences are as follow: *FZD10* (forward, 5'-AGCATCCCCAGAAAACTCAC-3'; reverse, 5'-AACACAACCAAGAAAAGCACC-3'), *FZD10m^{6}A site* (forward, 5'-CCTCCCCTGGGTTAACAAAT-3'; reverse, 5'-GGTGAAGGCCGGAGTCTATT-3'), *FOSL1* (forward, 5'-CTTGTGAACAGATCAGCCCGGA-3'; reverse, 5'-GTCGGTCAGTTCCTTCCTCC-3'), *CCND1* (forward, 5'-CCTGGTGAACAAGCTCAAGT-3'; reverse, 5'-GTGTTTGCGGATGATCTGTTTG-3'), β−2-microglobulin (*B2M*) (forward, 5'-GGCATTCCTGAAGCTGACA-3'; reverse, 5'-CTTCAATGTCGGATGGATGAAAC-3'), 18s (forward, 5'-AACTTTCGATGGTAGTCGCCG-3'; reverse, 5'-CCTTGGATGTGGTAGCCGTTT-3'), *FTO* (forward, 5'-GGAACCTTATTTTGGCATGGG-3'; reverse, 5'-GTCATCCTCACTTTCCTCTTCAG-3'), *ALKBH5* (forward, 5'-CCCTGCTCTGAAACCCAAG-3'; reverse, 5'-GTTCTCTTCCTTGTCCATCTCC-3'), *METTL3* (forward, 5'-GAAAGACTATCTCCTGGCACTC-3'; reverse, 5'-GTACCTTTGCTTGAACCGTG-3'), *METTL14* (forward, 5'-TTTCTCTGGTGTGGTTCTGG-3'; reverse, 5'-AAGTCTTAGTCTTCCCAGGATTG-3'), *HuR* (forward, 5'-GAGCTCAGAGGTGATCAAAGAC-3'; reverse, 5'-GCCCAAACCGAGAGAACAT-3'), *YTHDF2* (forward, 5'-CCTCCATTGGCTTCTCCTATTC-3'; reverse, 5'-GTTGCTCAGCTGTCCATAAGA-3'), *IGF2BP2* (forward, 5'-GAGCATATACAACCCGGAAAGA-3'; reverse, 5'-CCTCACGCAGCTTCTTCATA-3'). *B2M* or 18s were used as an internal control. Each sample was run in triplicate.

m^{6}A immunoprecipitation and sequencing, and measurement of total m^{6}A.

Cells were harvested at approximately 80% confluence. Total RNA was extracted and purified using RNeasy Midi Kit (QIAGEN, Cat. No. 75142). Purified total RNA was fragmented in freshly prepared RNA fragmentation buffer (10 mM Tris-HCl, pH 7.0, 10 mM $ZnCl_2$). The fragmented RNA was validated by RNA electrophoresis and 5 μg of fragmented RNA of each sample was preserved as input control for RNA-seq. 250 μg of fragmented RNA was subjected to m^{6}A immunoprecipitation using EpiMark® N6-Methyladenosine Enrichment Kit (NEB, Cat. No. E1610S) following manufacturer's instruction. Briefly, N6-Methyladenosine Antibody was coupled with protein G bead in reaction buffer for 30 min at 4°C, then fragmented RNA was incubated with the beads for 1 hour at 4°C. After incubation, the supernatant was discarded and the beads were washed twice in low salt reaction buffer and then washed twice in high salt reaction buffer. During this step the RNA containing the m^{6}A modification will remain on beads. Enriched m6A RNA was eluted with RLT buffer (QIAGEN, Cat. No. 75142) and concentrated by Dynabeads MyOne Silane (Life Technologies, Cat. No. 37002D). RNA was finally eluted with nuclease-free water and used for cDNA library preparation.

Library preparation and next generation sequencing were performed by The Wistar Institute Genomics Facility. Libraries for RNA-seq were prepared using ScriptSeq complete Gold kit (Epicentre) following the manufacturer's instructions. Libraries were pooled in equimolar concentration and then subjected to a 75 bp paired-end sequencing run on NextSeq 500, using Illumina's NextSeq 500 middle output sequencing kit. RNA-seq data was deposited in GEO database (Accession number: GSE119963).

For total m^{6}A measurement, total RNA was extracted from cells and m^{6}A content was measured by using EpiQuik m^{6}A RNA Methylation Quantification Kit (Epigentek, Cat. No. P-9005) according to the manufacturer's instructions.

Bioinformatic analysis

Raw sequencing data was aligned using *bowtie2* against hg19 version of the human genome and *RSEM* v1.2.12 software was used to estimate raw read counts and RPKM using Ensemble transcriptome. *EdgeR* (18) was used to estimate significance of differential expression between input RNA samples. Gene expression changes were considered significant if passed FDR<5% thresholds. *HOMER* was used to generate bigwig files and call m6A peaks (FDR<5%, at least 4 fold) in resistant vs parental cell lines and perform motif analysis. Most enriched consensus motif (AT**GGAC**TK, 73% of all FDR<5% peaks) was used for additional peak filtering. Only peaks that passed FDR<1% threshold and contained the motif were considered significant and used for further analysis. m6A signal fold difference in resistant vs parental cell lines was corrected by the difference in input RNA levels to account for overall gene expression changes effect on m6A signal. Genes that were significantly upregulated at least 2 fold and had a significantly higher m^{6}A peak of at least 2 fold in resistant vs parental cells in 5' or 3'UTR were reported. Normalized average signal around genes TSS and 3' UTR were derived from bigwig files using *bigWigAverageOverBed* tool from UCSC toolbox (19) with mean0 option using 20bp bins.

Colony formation assay.

Colony formation was performed as previously described (17). Briefly, Cells were cultured in 12-well, 24-well, or 96-well plates with different seeding number according to the growth rate. Medium was changed every three days with appropriate drug doses for 12 days or until control wells became confluent. Colonies were washed twice with PBS and fixed with 10% methanol and 10% acetic acid in distilled water. Fixed colonies were stained with 0.05% crystal violet. Analysis was performed using NIH ImageJ software.

Flow cytometry.

The Annexin V FITC and PI kit (Thermo Fisher, Cat. No. V13242) was used following the manufacturer's instructions. Briefly, cells were washed by PBS, trypsinized, and suspended in annexin V binding buffer. Cells were stained with annexin V and PI for 15 min and then analyzed. Analysis was performed using FlowJo version 7 software module.

For cell cycle analysis, the cells were fixed, treated with bovine RNase, and then stained with propidium iodide (Sigma-Aldrich) for 15 minutes at room temperature. Samples were subjected to analysis using the Becton-Dickinson LSR18 machine and FlowJo version 7 software module.

Wnt/β-catenin TCF/LEF reporter assay

The TOP FLASH reporter plasmid and RLSV40 Renilla plasmid were co-transfected into cells using Lipofectamine 3000. Following 48 hours, luciferase activity was measured using Dual-Luciferase Reporter Assay System (Promega) and Victor X3 2030 Multilabel Reader (Perkin Elmer) according to the manufacturer's instructions. Data was normalized based upon control Renilla luciferase activity. Each group was repeated in four times.

Dual Homologous Recombination (HR) and Non-Homologues End-Joining (NHEJ) reporter assay

The HR/NHEJ assay was performed as previously described (20). Briefly, cells were plated in 6-well plates at a 50% confluence one day before transfection. Cells were transfected with 500 ng of pLCN-DSB Repair Reporter (DDR), 500 ng of pCAGGS DRR mCherry Donor EF1 BFP plasmid, and 500 ng of pCBAsceI plasmid with Lipofectamine 2000. Seventy-two hours pCBAsceI plasmid or pCAGGS DRR mCherry Donor EF1 BFP plasmid alone were used as a control. The following plasmids were used: pLCN-DSB Repair Reporter (DDR) (Addgene Cat. No: 98895) pCAGGS DRR mCherry Donor EF1a BFP (Addgene Cat. No: 98896), and pCBASceI (Addgene Cat. No: 26477).

Xenograft PARP inhibitor resistant ovarian cancer mouse models.

The protocols were approved by the Wistar Institutional Animal Care and Use Committee (IACUC). 2×10^7 PARP inhibitor resistant PEO1 cells were suspended in 200 μL PBS : Matrigel (1:1) unilaterally injected subcutaneously into the right dorsal flank of 6–8 week-old female immunocompromised non-obese diabetic/severe combined immunodeficiency (NOD/SCID) gamma (NSG) mice. When the average tumor size reached ~100 mm^3, the mice were then randomized into four groups and treated with vehicle control, Olaparib (50

mg/kg), XAV939 (5 mg/kg) or a combination daily for 18 days. The indicated doses were determined based on previously studies (15,21). Olaparib was suspended in 10% 2-hydroxypropyl-β-cyclodextrin solvent (Sigma-Aldrich), and XAV939 was suspended in 4% DMSO/96% Corn oil (Sigma-Aldrich). Tumor size was measured three times a week. Tumor size was evaluated using the formula: tumor size (mm^3) = [$d^2 \times D$]/2, where d and D are the shortest and the largest diameter. At the end of the experiments, tumors were surgically dissected, and the weight of tumors were measured as a surrogate for tumor burden or followed for the survival of tumor bearing mice. The Wistar IACUC guideline was followed in determining the time for ending the survival experiments (tumor burden exceeds 10% of body weight).

Immunohistochemical staining.

Immunohistochemical staining was performed as described previously (15,17) on consecutive sections from xenografted tumors dissected from control or treated immunocompromised NSG female mice, using Dako EnVision+ system following the manufacturer's instructions. Expression of the stained markers was scored using a histologic score (H-score).

Statistical analysis.

All statistical analyses were conducted using GraphPad Prism 7 (GraphPad) for Mac OS. Experiments were repeated 3 times unless otherwise stated, and the representative results were shown. Quantitative data are expressed as mean ± S.E.M. For IC50 differences Z-test with 95% confidence intervals were used. A two-tailed t test was used to identify significant differences in comparisons unless otherwise stated. Combination index (CI) was analyzed by Compsyn software. CI value indicate: <1 synergism, =1 additive effect, and >1 antagonism. For all statistical analyses, the level of significance was set at 0.05.

Data availability

All sequencing data have been deposited in the Gene Expression Omnibus (GEO) under accession GSE119963.

Results

m^6A modified *FZD10* is upregulated in PARPi resistant cells.

To identify transcripts regulated by m^6A in PARPi resistance, we profiled m^6A distribution at the transcriptome level in *BRCA2*-mutated parental and PARPi resistant ovarian cancer PEO1 cells (15) by RNA immunoprecipitation followed sequencing using an anti-m^6A antibody (Fig. S1A–D). Consistent with previous reports (7–10), m^6A modification was enriched in both 3' and 5' UTR regions at the transcriptome level (Fig. 1A). However, the overall m^6A pattern in the transcriptomes was not significantly different between parental and resistant cells (Fig. 1A). Likewise, there was no significant difference in total m^6A modified mRNA between parental and resistant cells (Fig. S1E).

We next analyzed the genes that were differentially modified by m^6A between parental and resistant cells. The top gene whose m^6A modification was increased in PARPi resistant cells

was *FZD10* (Fig. 1A). m^6A levels at the 3' UTR region of the *FZD10* mRNA was significantly increased in resistant cells (Fig. 1B). The increase in m^6A modified *FZD10* was confirmed by anti-m^6A immunoprecipitation and qRT-PCR analysis of the m^6A immunoprecipitated RNAs (Fig. 1B). The increase in m^6A modified *FZD10* correlated with an increase in *FZD10* mRNA in resistant cells (Fig. 1C). These results suggest that m^6A modification may stabilize *FZD10* mRNA. Consistently, we observed an increase in FZD10 protein in resistant cells (Fig. 1C). Indeed, RNA stability analysis revealed that FZD10 mRNA is significantly stabilized in resistant cells (Fig. 1D). However, there is no significant difference in FZD10 protein stability between parental and resistant PEO1 cells (Fig. S1F–G). Together, we conclude that m^6A modification is increased in the 3' UTR region of the *FZD10* gene when the *BRCA2*-mutated PEO1 cells developed resistance to PARP inhibitors.

Inhibition of FZD10 and Wnt signaling overcomes PARPi resistance.

Given that FZD10 is a receptor in the canonical Wnt/β-catenin signaling (4), we next determined whether the Wnt/β-catenin signaling is altered in PARPi resistant cells. Notably, nuclear β-catenin levels were increased in PARPi resistant cells and this correlates with an increase in the expression of the Wnt/β-catenin target genes in these cells (Fig. 2A and S2A and B). Consistently, the TCF/LEF reporter activity was higher in resistant cells (Fig. 2A). To determine the role of the upregulated FZD10 in PARPi sensitivity in the resistant cells, FZD10 was knocked down in PARPi resistant cells (Fig. 2B). FZD10 knockdown decreased the Wnt/β-catenin target gene expression in PARPi resistant cells (Fig. S2C and D). This correlated with a decrease in the IC_{50} of two different PARP inhibitors Olaparib and Rucaparib in FZD10 knockdown cells (Fig. 2B and S2E). Consistently, inhibitors of the Wnt/β-catenin signaling, namely XAV939 (22) and pyrvinium pamoate (23), were more effective in suppressing the growth of PARPi resistant cells (Fig. 2C).

We next explored changes in HR and non-homologous end joining (NHEJ) activities, two alternating DNA double strand break repairing pathways using a dual HR and NHEJ reporter assay (20) (Fig. 2D). Consistent with previous reports (1), we observed a significant increase in HR activity in PARPi resistant cells (Fig. S2F). As a control, NHEJ activity was not significantly affected in PARPi resistant cells (Fig. S2G). However, the observed increase in HR activity was not due to an increase in S phase of the cell cycle and FZD10 knockdown did not significantly affect S phase of the cell cycle in the resistant cells (Fig. S2H–I). Notably, FZD10 knockdown significantly decreased HR activity without affecting NHEJ activity (Fig. 2D and S2J). Together, we conclude that inhibition of FZD10 suppresses the Wnt/β-catenin signaling and sensitizes the PARPi resistant cells to PARPi.

Downregulation of FTO and ALKBH5 contributes to FZD10 mRNA upregulation.

Since *FZD10* m^6A upregulation contributes to FZD10 upregulation, we next determined the changes in expression of m^6A methyltransferase and demethylase in parental and resistant cells. Notably, both m^6A demethylases *FTO* and *ALKBH5* are downregulated in resistant cells compared with parental cells (Fig. 3A). As a control, the expression of m^6A methyltransferase *METTLE14* and *METTLE3* expression was downregulated in resistant cells (Fig. S3A). Given FZD10 m^6A modification was increased in resistant cells, we determined whether downregulation of FTO and/or ALKBH5 is sufficient to upregulate

FZD10 expression (Fig. S3B). Indeed, knockdown of either ALKBH5 or FTO in PEO1 parental cells increased the expression of FZD10 and a combination of ALKBH5 and FTO knockdown further increased FZD10 expression (Fig. 3B). This suggests that downregulation of both ALKBH5 and FTO contributes to FZD10 upregulation. Similar upregulation of FZD10 by knockdown of ALKBH5 and FTO was also obtained in *BRCA1*-mutated UWB1.289 ovarian cancer cells (Fig. S3C–E), suggesting that the observed effects are not a cell line-specific effect. Notably, the observed FZD10 upregulation correlates with an increase in Wnt target gene expression and an increase HR activity without affecting NHEJ activity (Fig. 3C and S3F–H), which was accompanied by a decrease in sensitivity to Olaparib (Fig. 3D). Conversely, ectopic expression of ALKBH5 and FTO in the resistant cells increased Olaparib sensitivity (Fig. S3I–J). We next determined the expression of the m^6A readers namely *HuR*, *IGF2BP2* and *YTHDF2* (11–13) in parental and resistant cells. Notably, expression of both *YTHDF2* and *HuR* was decreased in the resistant cells, while *IGF2BP2* expression was increased in the resistant cells (Fig. S3K). In addition, knockdown of any of the readers decreased *FZD10* expression (Fig. S3L–N). Given that *YTHDF2* promotes the decay while *HuR* and *IGF2BP2* stabilize the m^6A modified mRNA (11–13), these results suggest that *IGF2BP2* plays a role downstream of the m^6A modified *FZD10* mRNA. Together, we conclude that downregulation of m^6A demethylases ALKBH5 and FTO contributes to FZD10 upregulation in PARPi resistant cells.

Wnt signaling inhibitor XAV939 and Olaparib are synergistic in suppressing PARPi resistant cells *in vitro* and *in vivo*.

We next determined that Olaparib and XAV939 were synergistic in suppressing the growth of PARPi resistant cells (Fig. 4A). In contrast, there was no synergy between Olaparib and XAV939 in parental cells (Fig. 4A). Notably, XAV939 alone induced apoptosis of PARPi resistant cells as evidenced by an increase in Annexin V positive cells and an upregulation of cleaved PARP p85 and cleaved caspase 3 (Fig. 4B). As a control, Olaparib alone did not affect markers of apoptosis in PARPi resistant cells. However, a combination of XAV939 and Olaparib significantly increased markers of apoptosis compared with XAV939 alone (Fig. 4B). This is consistent with the observed synergy between Olaparib and XAV939 in suppressing the growth of PARPi resistant cells (Fig. 4A). In contrast, XAV939 did not significantly increase apoptosis induced by Olaparib in parental PEO1 cells (Fig. S4A–B).

We next transplanted PARPi resistant PEO1 cells into NSG mice. When the average xenograft tumor size reached ~100 mm^3, mice were randomized into four groups with 12 mice in each of the groups for the following treatments: vehicle control, Olaparib, XAV939 and a combination of Olaparib and XAV939. After 18 days of treatment, half of the mice from each of the groups were euthanized (Fig. 4C). Compared with vehicle controls, XAV939 significantly suppressed the growth of the xenografted PARPi resistant tumors (Fig. 4C). Notably, a combination of Olaparib and XAV939 exhibited significantly greater tumor suppressive effect as compared to either XAV939 or Olaparib alone (Fig. 4C and S4C). The doses of Olaparib and XAV939 used in this study did not significantly affect the body weight of treated mice (Fig. S4D), suggesting that effective combination doses can be achieved without added toxicity. XAV939 alone significantly improved the survival of mice bearing PARPi resistant tumors (Fig. 4C). However, the survival of mice treated with a

combination of XAV939 and Olaparib was significantly longer than those treated with XAV939 alone (Fig. 4C).

We next performed IHC staining for Ki67, a cell proliferation marker, and cleaved caspase 3, an apoptosis marker, on the consecutive sections of the dissected tumors (Fig. 4D). Both XAV939 alone and a combination of XAV939 and Olaparib significantly decreased Ki67 expression and increased cleaved caspase 3 expression (Fig. 4D). In addition, XAV939 alone or in combination with Olaparib significantly decreased the expression of the Wnt/β-catenin target genes such as *FOSL1* and *CCND1* (Fig. 4D). Taken together, we conclude that XAV939 synergizes with Olaparib in suppressing the growth of PARPi resistant tumors. This activity correlates with a decrease in cell proliferation and an increase in apoptosis, accompanied by downregulation in Wnt/β-catenin signaling by XAV939.

Discussion

Here we show that downregulation of m^6A erasers FTO and ALKBH5 contribute to PARPi resistance by increasing m^6A modification in *FZD10* mRNA to upregulate Wnt signaling. The current study focuses on FZD10 regulated Wnt signaling due to the fact that FZD10 showed the highest degree of increase in m^6A modification. However, it is possible that FTO and ALKBH5 may also contribute to PARPi resistance through regulating m^6A modification in genes implicated in Wnt-independent pathways.

Restoration of HR activity by mechanisms such as genetic reversion of truncating mutations (1,24) contributes to PARPi resistance in *BRCA1/2*-mutated cancer cells. Here we show that knockdown of FZD10 decreases HR activity in PARPi resistant cells while upregulation of FZD10 increases HR activity in parental cells. Thus, FZD10 regulated Wnt pathway contributes to an increase in HR activity. These results suggest that Wnt signaling is a novel regulator of HR activity. This is consistent with a preprint finding that Wnt signaling upregulates HR activity (25). Interestingly, the observed upregulation of HR activity is independent of *BRCA2* genetic reversion (25).

In summary, our findings revealed that m^6A modification represents a novel mechanism of PARPi resistance. In addition, we showed that upregulation of Wnt signaling at least in part contributes to m^6A modification mediated PARPi resistance. Our results suggest that inhibition of the Wnt/β-catenin pathway represents a potential strategy to overcome PARPi resistance.

Supplementary Material

Refer to Web version on PubMed Central for supplementary material.

Acknowledgements

This work was supported by US National Institutes of Health grants (R01CA160331, R01CA163377, R01CA202919 and P50CA228991 to R. Z., and R50CA211199 to A.V.K.) and US Department of Defense (OC140632P1 and OC150446 to R. Z.). The Honorable Tina Brozman Foundation for Ovarian Cancer Research (to R.Z.) and Ovarian Cancer Research Alliance (Collaborative Research Development Grant to R.Z., and Ann and Sol Schreiber Mentored Investigator Award to S.W.). Support of Core Facilities was provided by Cancer Centre Support Grant (CCSG) CA010815 to The Wistar Institute.

References

1. Lord CJ, Ashworth A. PARP inhibitors: Synthetic lethality in the clinic. Science 2017;355:1152–8 [PubMed: 28302823]
2. Konstantinopoulos PA, Matulonis UA. PARP Inhibitors in Ovarian Cancer: A Trailblazing and Transformative Journey. Clin Cancer Res 2018;24:4062–5 [PubMed: 29871906]
3. Nusse R, Clevers H. Wnt/beta-Catenin Signaling, Disease, and Emerging Therapeutic Modalities. Cell 2017;169:985–99 [PubMed: 28575679]
4. MacDonald BT, He X. Frizzled and LRP5/6 receptors for Wnt/beta-catenin signaling. Cold Spring Harb Perspect Biol 2012;4
5. Salic A, Lee E, Mayer L, Kirschner MW. Control of beta-catenin stability: reconstitution of the cytoplasmic steps of the wnt pathway in Xenopus egg extracts. Mol Cell 2000;5:523–32 [PubMed: 10882137]
6. Yue Y, Liu J, He C. RNA N6-methyladenosine methylation in post-transcriptional gene expression regulation. Genes Dev 2015;29:1343–55 [PubMed: 26159994]
7. Dominissini D, Moshitch-Moshkovitz S, Schwartz S, Salmon-Divon M, Ungar L, Osenberg S, et al. Topology of the human and mouse m6A RNA methylomes revealed by m6A-seq. Nature 2012;485:201–6 [PubMed: 22575960]
8. Meyer KD, Saletore Y, Zumbo P, Elemento O, Mason CE, Jaffrey SR. Comprehensive analysis of mRNA methylation reveals enrichment in 3' UTRs and near stop codons. Cell 2012;149:1635–46 [PubMed: 22608085]
9. Meyer KD, Patil DP, Zhou J, Zinoviev A, Skabkin MA, Elemento O, et al. 5' UTR m(6) A Promotes Cap-Independent Translation. Cell 2015;163:999–1010 [PubMed: 26593424]
10. Zhou J, Wan J, Gao X, Zhang X, Jaffrey SR, Qian SB. Dynamic m(6) A mRNA methylation directs translational control of heat shock response. Nature 2015;526:591–4 [PubMed: 26458103]
11. Zhang S, Zhao BS, Zhou A, Lin K, Zheng S, Lu Z, et al. m(6) A Demethylase ALKBH5 Maintains Tumorigenicity of Glioblastoma Stem-like Cells by Sustaining FOXM1 Expression and Cell Proliferation Program. Cancer Cell 2017;31:591–606 e6 [PubMed: 28344040]
12. Huang H, Weng H, Sun W, Qin X, Shi H, Wu H, et al. Recognition of RNA N(6)-methyladenosine by IGF2BP proteins enhances mRNA stability and translation. Nat Cell Biol 2018;20:285–95 [PubMed: 29476152]
13. Wang X, Lu Z, Gomez A, Hon GC, Yue Y, Han D, et al. N6-methyladenosine-dependent regulation of messenger RNA stability. Nature 2014;505:117–20 [PubMed: 24284625]
14. Deng X, Su R, Feng X, Wei M, Chen J. Role of N(6)-methyladenosine modification in cancer. Curr Opin Genet Dev 2018;48:1–7 [PubMed: 29040886]
15. Karakashev S, Zhu H, Yokoyama Y, Zhao B, Fatkhutdinov N, Kossenkov AV, et al. BET Bromodomain Inhibition Synergizes with PARP Inhibitor in Epithelial Ovarian Cancer. Cell Rep 2017;21:3398–405 [PubMed: 29262321]
16. Aird KM, Iwasaki O, Kossenkov AV, Tanizawa H, Fatkhutdinov N, Bitler BG, et al. HMGB2 orchestrates the chromatin landscape of senescence-associated secretory phenotype gene loci. J Cell Biol 2016;215:325–34 [PubMed: 27799366]
17. Bitler BG, Wu S, Park PH, Hai Y, Aird KM, Wang Y, et al. ARID1A-mutated ovarian cancers depend on HDAC6 activity. Nat Cell Biol 2017;19:962–73 [PubMed: 28737768]
18. Robinson MD, McCarthy DJ, Smyth GK. edgeR: a Bioconductor package for differential expression analysis of digital gene expression data. Bioinformatics 2010;26:139–40 [PubMed: 19910308]
19. Kent WJ, Zweig AS, Barber G, Hinrichs AS, Karolchik D. BigWig and BigBed: enabling browsing of large distributed datasets. Bioinformatics 2010;26:2204–7 [PubMed: 20639541]
20. Arnoult N, Correia A, Ma J, Merlo A, Garcia-Gomez S, Maric M, et al. Regulation of DNA repair pathway choice in S and G2 phases by the NHEJ inhibitor CYREN. Nature 2017;549:548–52 [PubMed: 28959974]

21. Wu DW, Lin PL, Cheng YW, Huang CC, Wang L, Lee H. DDX3 enhances oncogenic KRASinduced tumor invasion in colorectal cancer via the betacatenin/ZEB1 axis. Oncotarget 2016;7:22687–99 [PubMed: 27007150]

22. Huang SM, Mishina YM, Liu S, Cheung A, Stegmeier F, Michaud GA, et al. Tankyrase inhibition stabilizes axin and antagonizes Wnt signalling. Nature 2009;461:614–20 [PubMed: 19759537]

23. Thorne CA, Hanson AJ, Schneider J, Tahinci E, Orton D, Cselenyi CS, et al. Small-molecule inhibition of Wnt signaling through activation of casein kinase 1alpha. Nat Chem Biol 2010;6:829–36 [PubMed: 20890287]

24. Stover EH, Konstantinopoulos PA, Matulonis UA, Swisher EM. Biomarkers of Response and Resistance to DNA Repair Targeted Therapies. Clin Cancer Res 2016;22:5651–60 [PubMed: 27678458]

25. Yamamoto TM, McMellen A, Watson ZL, Aguilera J, Sikora MJ, Ferguson R, et al. Targeting Wnt Signaling to Overcome PARP Inhibitor Resistance. bioRxiv

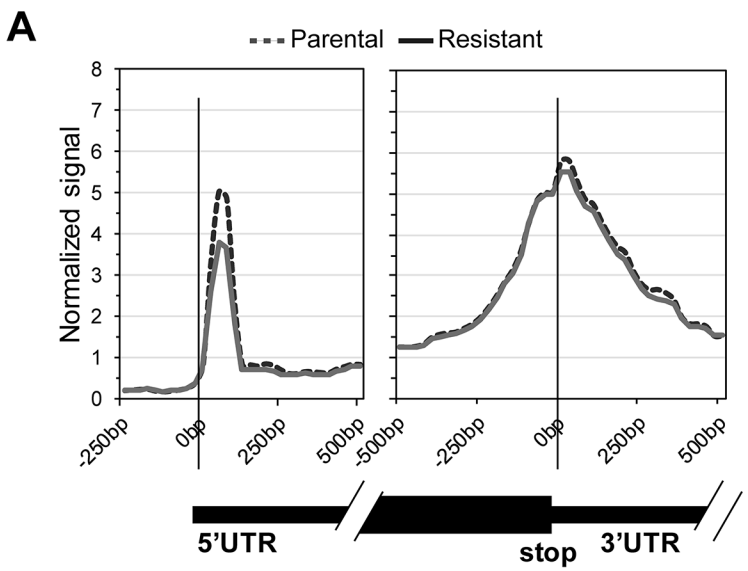

Resistant/Parental m^{6}A	UTR	input	Gene
19.5	3 '	2.2	FZD10
15.1	3 '	2.2	GOLGA7
12.1	3 '	2.1	KLHDC8B
7.7	3 '	2.2	ARNT2
5.9	3 '	2.2	NSF
5.9	3 '	2.2	SDC2
5.5	5 '	2.0	HOXC6
5.3	3 '	2.8	HCN2
5.2	5 '	2.5	GNG11
4.4	5 '	3.3	RMI2
4.4	5 '	4.3	BGN
4.1	5 '	3.6	NWD1
4.0	3 '	3.7	COL5A1
3.4	5 '	3.2	TGFB2
3.0	3 '	2.8	MSRB3

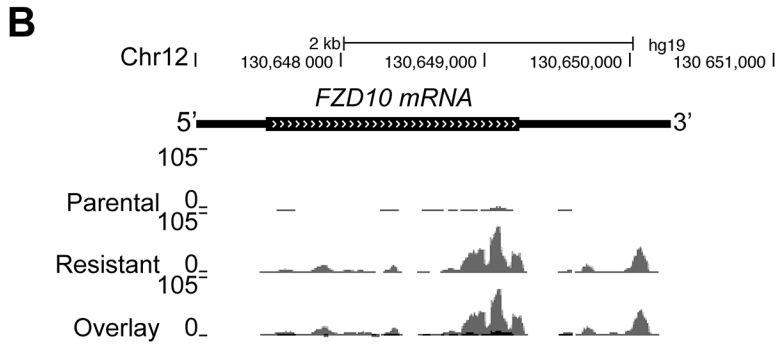

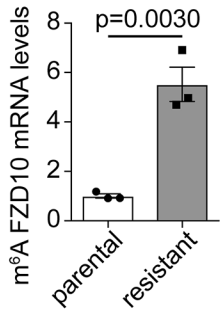

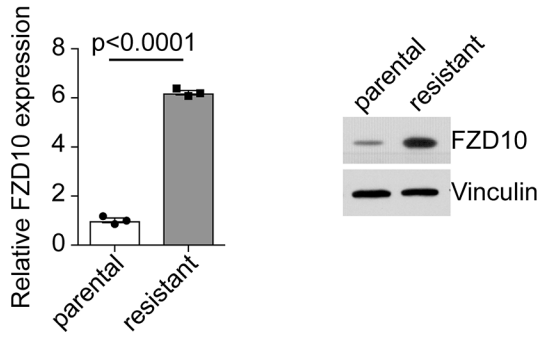

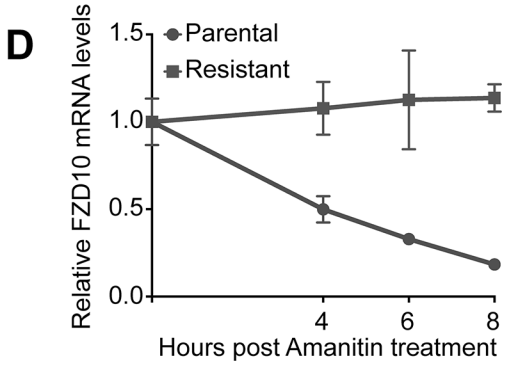

Figure 1. m^{6}A modification contributes to FZD10 upregulation in PARPi resistant cells.

(**A**) Megagene profiles depicting global changes in m^{6}A binding surrounding 5' and 3' end UTRs in parental and PARPi resistant PEO1 cells. Shown is a list of genes that exhibited at least a 3-fold increase in m^{6}A modification in either 5' or 3' end UTRs. (**B**) Tracks of m^{6}A sequence of *FZD10* mRNA in parental and PARPi resistant PEO1 cells, which was validated using an anti-m^{6}A antibody immunoprecipitation followed by qRT-PCR analysis. (**C**) Expression of *FZD10* mRNA and protein in parental and PARPi resistant PEO1 cells determined by qRT-PCR and immunoblotting. (**D**) *FZD10* mRNA stability is increased in

PARPi resistant PEO1 cells. Data represent mean ± S.E.M. of three independent experiments.

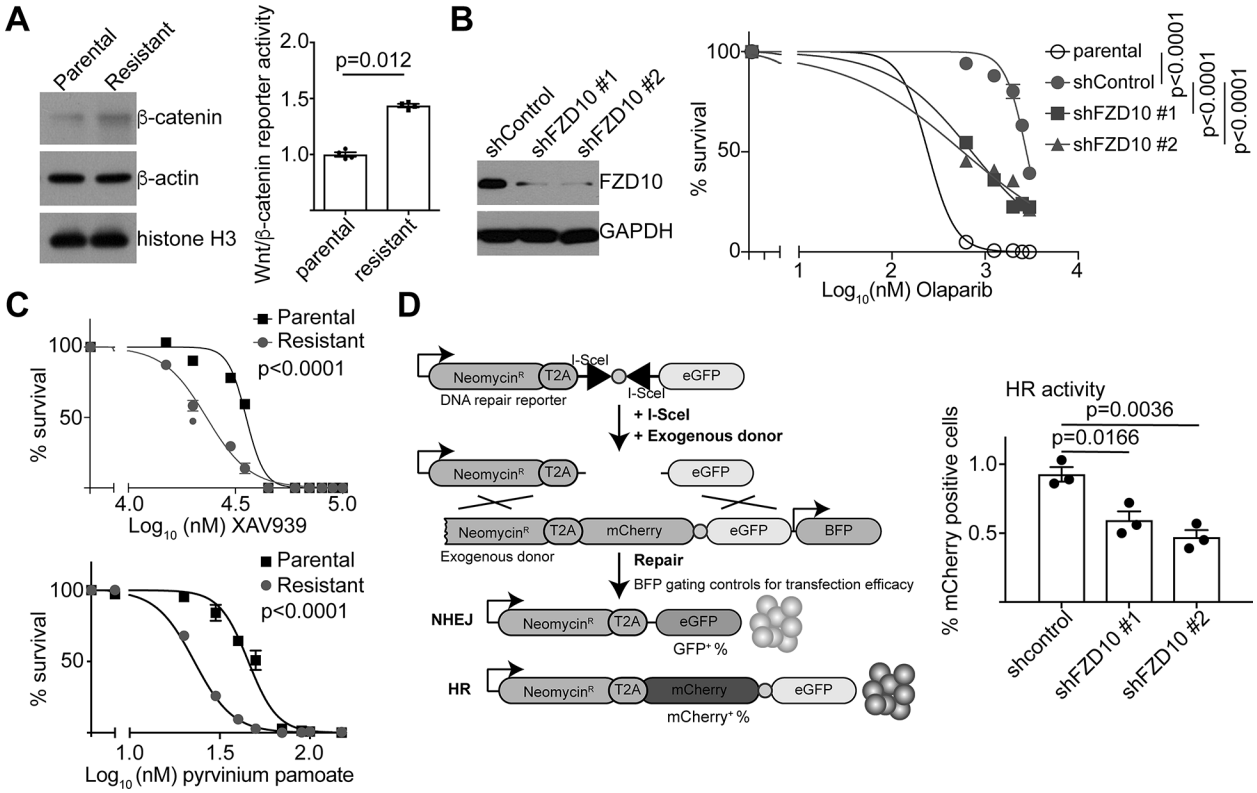

Figure 2. FZD10 contributes to PARPi resistance by upregulating the Wnt/β-catenin pathway and HR DNA repair activity.

(**A**) Expression of nuclear β-catenin, β-actin and histone H3 was determined by immunoblotting. Wnt/β-catenin signalling in PARPi resistant PEO1 cells was determined by a TCF/LEF dual luciferase reporter assay (n=4 independent experiments). (**B**) PARPi resistant PEO1 cells expressing shFZD10 or control were validated for the knockdown of FZD10 by immunoblotting and examined for Olaparib dose response curves. (**C**) Dose response curves of Wnt signalling inhibitors XAV939 and pyrvinium pamoate in parental and PARPi resistant PEO1 cells. (**D**) Knockdown of FZD10 decreased HR activity as determined by the dual HR and NHEJ reporter assay as shown in the schematics on the left (20). Data represent mean ± S.E.M. of three independent experiments unless otherwise specified.

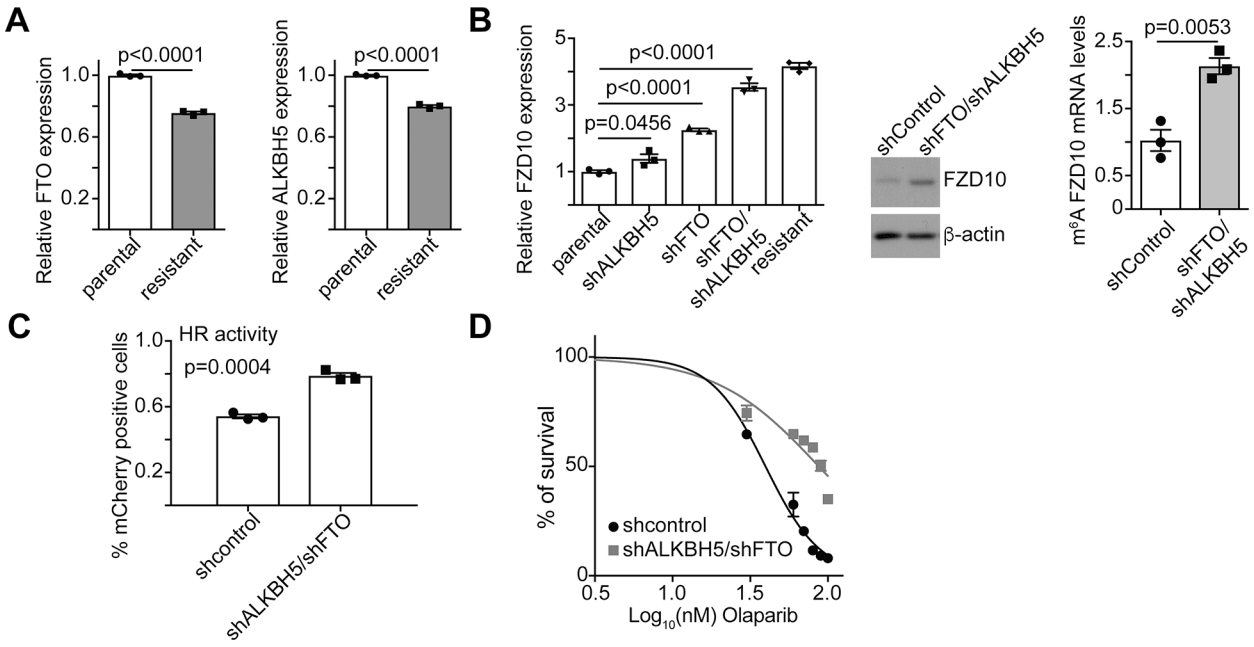

Figure 3. Downregulation of m^{6}A demethylases ALKBH5 and FTO increases m^{6}A modified FZD10 and decreases PARPi sensitivity.

(**A**) Expression of *FTO* and *ALKBH5* in parental control and PARPi resistant PEO1 cells determined by qRT-PCR. (**B**) Expression of *FZD10* determined by qRT-PCR in parental PEO1 cells expressing the indicated shRNAs to the *ALKBH5* gene (shALKBH5) and/or the *FTO* gene (shFTO) determined by qRT-PCR. FZD10 expression in PARPi resistant PEO1 cells was used as a positive control. In the middle panel, FZD10 protein expression in PEO1 parental cells expressing the indicated shRNAs or control was determined by immunoblotting. The m^{6}A modified *FZD10* mRNA level in the indicated cells was quantified by immunoprecipitation of mRNA using an anti-m^{6}A antibody followed by qRT-PCR in the right. (**C**) Knockdown of ALKBH5 and FTO increased HR activity. (**D**) Dose response curves of Olaparib in parental PEO1 cells expressing the indicated shRNAs. Data represent mean ± S.E.M. of three independent experiments.

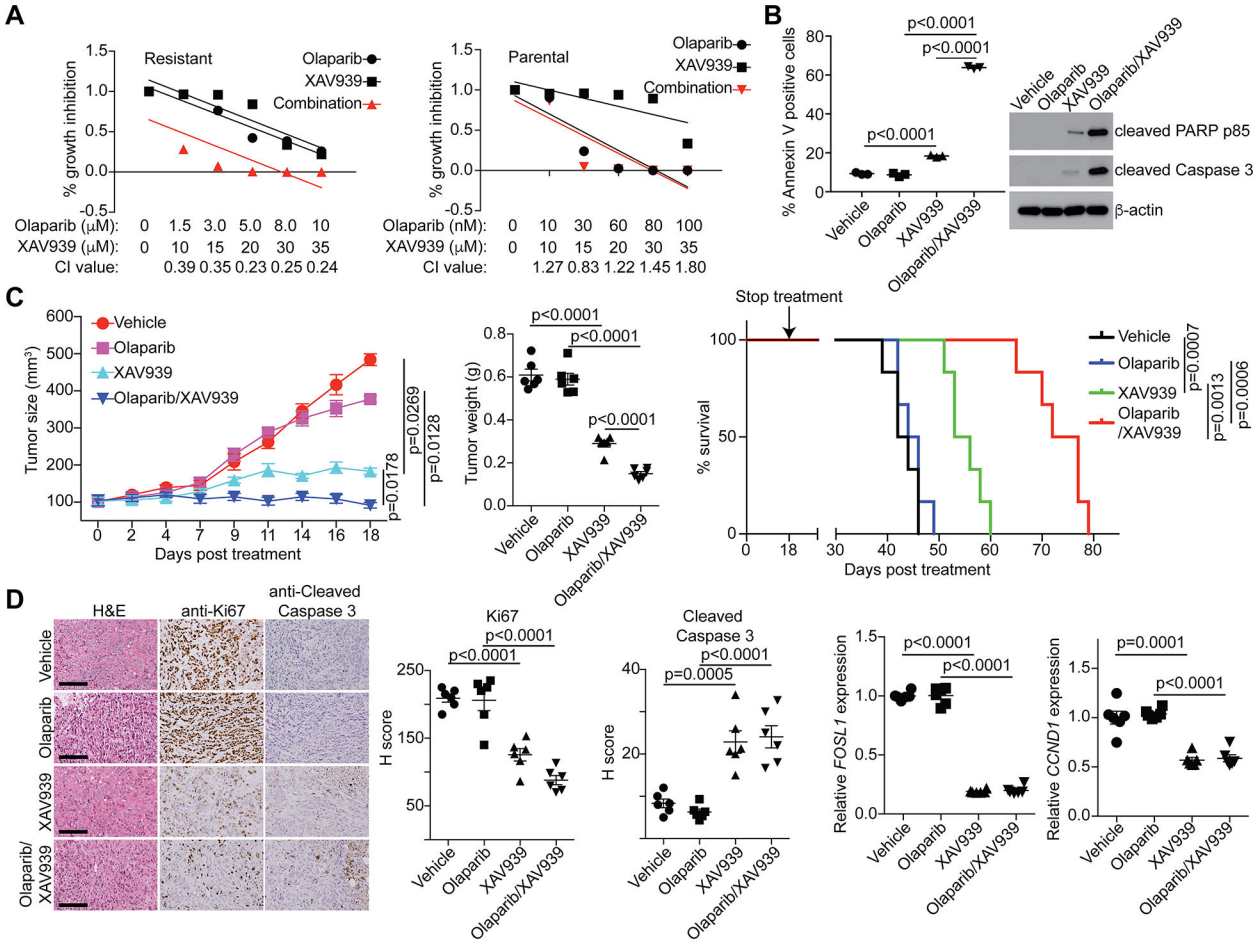

Figure 4. Wnt inhibitor XAV939 and PARPi Olaparib are synergistic in suppressing PARPi resistant tumors *in vivo*.

(**A**) Synergy analysis of Olaparib and XAV939 in PARPi resistant and parental control PEO1 cells (n=4). (**B**) Apoptosis in the PARPi resistant PEO1 cells treated with 0.5 μM Olaparib, 20 μM XAV939, or a combination were quantified by Annexin V staining or immunoblotting. (**C**) The growth of tumors formed by PARPi resistant PEO1 cells in the indicated treatment groups was measured at the indicated time points in left panel. The weight of the dissected tumors was measured as a surrogate for tumor burden in middle panel. The survival was plotted in the Kaplan-Meier survival curves in right panel. *P*-value was calculated by log-rank test. (**D**) In the left panel, serial sections of the dissected tumors from the indicated treatment groups were subjected to immunohistochemical staining using antibodies against Ki67 or cleaved caspase 3. Scale bar = 50 μm. In the middle panel, the histological score (H-score) of Ki67 and cleaved caspase 3 was calculated. In the right panel, the expression of Wnt target genes *FOSL1* and *CCND1* was determined by qRT-PCR (n=6). Data represent mean ± S.E.M.